Frontiers of Information Technology & Electronic Engineering
www.jzus.zju.edu.cn; engineering.cae.cn; www.springerlink.com
ISSN 2095-9184 (print); ISSN 2095-9230 (online)
E-mail: jzus@zju.edu.cn

Correspondence:

Effective degree of freedom for near-field plane-based XL-MIMO with tri-polarization*

Zhe WANG†1,2, Jiayi ZHANG†‡1, Wenhui YI[1], Huahua XIAO[3], Dusit NIYATO[2], Bo AI[1]

[1]*School of Electronic and Information Engineering, Beijing Jiaotong University, Beijing 100044, China*

[2]*College of Computing and Data Science, Nanyang Technological University, Singapore 639798, Singapore*

[3]*State Key Laboratory of Mobile Network and Mobile Multimedia Technology, ZTE Corporation, Shenzhen 518057, China*

†E-mail: zhewang_77@bjtu.edu.cn; jiayizhang@bjtu.edu.cn

Received Mar. 7, 2024; Revision accepted Aug. 8, 2024; Crosschecked Nov. 28, 2024

https://doi.org/10.1631/FITEE.2400167

In this paper we study the effective degree of freedom (EDoF) for extremely large-scale multiple-input multiple-output (XL-MIMO) systems. We consider two XL-MIMO hardware designs, uniform planar array (UPA) based and continuous aperture (CAP) based XL-MIMO, as well as two representative near-field channel models: scalar Green function based and dyadic Green function with triple polarization based models. First, for UPA-based XL-MIMO with a discrete array aperture, we evaluate the EDoF performance by applying discrete channel matrices generated by the scalar or dyadic Green channel model. Then, for CAP-based XL-MIMO, a tailored EDoF performance evaluation framework for a two-dimensional (2D) CAP plane based system is constructed by leveraging asymptotic analysis and extending the analysis approaches for a one-dimensional (1D) CAP line segment based system. This framework incorporates the triple-polarized auto-correlation kernel function, which can efficiently capture the impact of multiple polarization on the EDoF performance. Numerical results show that, with an increase in the number of antennas, the UPA-based XL-MIMO system can achieve an EDoF performance close to the EDoF performance for the CAP plane based XL-MIMO system. Moreover, the EDoF performance can be enhanced by the multiple polarization in channels and increased physical size of the transceiver.

1 Introduction

With the rapid development of wireless communications, the anticipated beyond fifth-generation (B5G) and sixth-generation (6G) wireless communication networks have been widely studied (Zhang JY et al., 2020; Tataria et al., 2021; You XH et al., 2021). Concurrently, the escalation in communication demands and the variety of application scenarios have introduced substantial challenges (Huang et al., 2021; Ouyang et al., 2022; Du et al., 2023; Zheng et al., 2023; Sun et al., 2024). To tackle these challenges, many promising enabling technologies have been widely applied in wireless communication (Letaief et al., 2019; Zhang JY et al., 2020;

‡ Corresponding author

* Project supported by the National Natural Science Foundation of China (No. 62221001), the National Research Foundation, Singapore, and Infocomm Media Development Authority under its Future Communications Research & Development Programme, the Defence Science Organisation (DSO) National Laboratories under the AI Singapore Programme (Nos. CP-NTU-RG-2022-010 and FCP-ASTAR-TG-2022-003), the Singapore Ministry of Education (MOE) Tier 1 (No. RG87/22), and the NTU Centre for Computational Technologies in Finance (NTU-CCTF)

Electronic supplementary materials: The online version of this article (https://doi.org/10.1631/FITEE.2400167) contains supplementary materials, which are available to authorized users

ORCID: Zhe WANG, https://orcid.org/0000-0001-5745-7640; Jiayi ZHANG, https://orcid.org/0000-0003-2434-4329

Chen et al., 2021; Du et al., 2024; Gong et al., 2024; Shi et al., 2024; Wang et al., 2024b). Among these technologies, XL-MIMO technology holds high expectations (Cui et al., 2023; Lu et al., 2023; Lei et al., 2024a, 2024b; Tang et al., 2024; Wang et al., 2024b).

MIMO technology has been viewed as an important enabler of wireless communication networks since the advent of fourth-generation (4G) wireless communication networks (Marzetta, 2010; Björnson et al., 2019, 2024; Gan et al., 2021; Zhang JY et al., 2021; Chen et al., 2023). As an evolution of conventional massive MIMO (mMIMO) technology, XL-MIMO employs an extremely large number of antennas, for example, thousands, even tens of thousands, of antennas (Lu et al., 2023; Xu et al., 2023; Wang et al., 2024b). The extremely large array aperture in XL-MIMO necessitates the consideration of near-field spherical wave characteristics, which are typically neglected in conventional mMIMO due to the small or moderate array aperture (You CS et al., 2023; Liu YW et al., 2024; Liu ZH et al., 2024; Wang et al., 2024b; Xu et al., 2024). Mainly three promising XL-MIMO hardware designs, i.e., uniform linear array (ULA) based (Cui and Dai, 2022), UPA-based (Lu and Zeng, 2022), and CAP-based (Zhang ZJ and Dai, 2023) XL-MIMO designs, have attracted significant attention (Liu ZL et al., 2024; Wang et al., 2024a, 2024b).

To fully explore the benefits of XL-MIMO technology, the performance limit analysis for XL-MIMO systems is vital. Several works have studied the degree of freedom (DoF) for near-field XL-MIMO systems (Yuan et al., 2022; Jiang and Gao, 2023; Ouyang et al., 2023; Xie et al., 2023). Ouyang et al. (2023) reviewed three DoF-related performance metrics and compared their characteristics and insights, and provided important guidelines for DoF performance analysis for near-field XL-MIMO systems. Among the various performance metrics, EDoF has garnered significant research interest. EDoF is an approximate mathematical solution for the number of dominant singular values of the channel (Ouyang et al., 2023). Note that EDoF can be directly related to the slope of the capacity performance of systems, which is intuitive in depicting the capacity performance. Based on the scalar Green function based channel model (we call it the scalar Green channel model in the following briefly), Jiang and Gao (2023) and Xie et al. (2023) studied EDoF for both the ULA-based and 1D CAP line segment systems. Notably, the EDoF expressions in Xie et al. (2023) were computed in a novel closed form. Moreover, Yuan et al. (2022) analyzed the EDoF performance for the UPA systems with the dyadic Green function based channel model (we call it the dyadic Green channel model in the following briefly). Note that the dyadic Green function captures triple polarization, which is more accurate for describing near-field electromagnetic (EM) characteristics compared with the scalar Green channel model. However, existing research on the EDoF analysis of CAP systems has been limited to scenarios involving the 1D CAP line segment.

In practice, 2D plane based XL-MIMO systems are extensively researched and advocated (Wang et al., 2024b). The UPA-based system with the discrete array aperture and the 2D CAP plane based system with the continuous array aperture are regarded as two promising plane-based XL-MIMO hardware designs. It is crucial to assess the EDoF performance of these designs and explore their respective performance limits. Note that the CAP plane based system can be regarded as a special case of the UPA-based system by considering an infinite number of antennas while maintaining the array size. However, the performance analysis for the CAP- and UPA-based systems is carried out in the continuous integral dimension and the discrete matrix dimension (Ouyang et al., 2023), respectively. Conducting further studies to analyze the EDoF performance of 2D CAP plane systems and compare their performance with that of UPA systems is both interesting and essential.

To address the research gap, in this study, we analyze the EDoF performance of both UPA-based and 2D CAP plane based XL-MIMO systems with both the scalar and dyadic Green channels. For UPA-based XL-MIMO, we evaluate the EDoF performance by leveraging the discrete channel matrices for both the scalar Green and the dyadic Green channels. Moreover, we propose a novel EDoF performance analysis framework specifically for the 2D CAP plane systems over the dyadic Green channel, with the aid of asymptotic analysis for the EDoF performance analysis framework for the UPA system. This framework embraces the auto-correlation kernel with triple polarization considered, capturing

the impact of multiple polarization on EDoF performance. Finally, numerical results are provided to compare the performance of the UPA system and 2D CAP plane system, and to evaluate the effects of polarization and the physical size of the transceiver.

2 System model

In this section, we introduce the system model of the UPA-based and CAP plane based XL-MIMO systems. Specifically, the system features and channel models are discussed.

2.1 UPA-based XL-MIMO

2.1.1 System feature

We first investigate the UPA-based XL-MIMO as illustrated in Fig. 1, where both a transmitter and a receiver are equipped with a UPA with point antenna elements. The transmitting plane lies in the XY plane with its left-bottom point being the origin. The transmitting array consists of M_{V} antennas per column and M_{H} antennas per row. Thus, the transmitter is equipped with $M = M_{\mathrm{H}}M_{\mathrm{V}}$ antennas in total. The antenna spacings in the vertical column and horizontal row are $\Delta_{\mathrm{t,V}}$ and $\Delta_{\mathrm{t,H}}$, respectively, and the vertical and horizontal side lengths for the transmitter are $L_{\mathrm{t,V}} = M_{\mathrm{V}}\Delta_{\mathrm{t,V}}$ and $L_{\mathrm{t,H}} = M_{\mathrm{H}}\Delta_{\mathrm{t,H}}$, respectively. For the convenience of analysis, we define the antenna index row by row as $m \in \{1, 2, \ldots, M\}$ from left to right and from bottom to top. Thus, the location of the m^{th} antenna element at the transmitter can be denoted as $\boldsymbol{r}_{\mathrm{t},m} = [o(m)\Delta_{\mathrm{t,H}}, j(m)\Delta_{\mathrm{t,V}}, 0]^{\mathrm{T}} \in \mathbb{R}^3$, where $o(m) = \mathrm{mod}(m-1, M_{\mathrm{H}})$ and $j(m) = \lfloor (m-1)/M_{\mathrm{H}} \rfloor$ are the indices of the horizontal and vertical directions for the m^{th} antenna element at the transmitter, respectively. Furthermore, V_{T} denotes the transmitting volume.

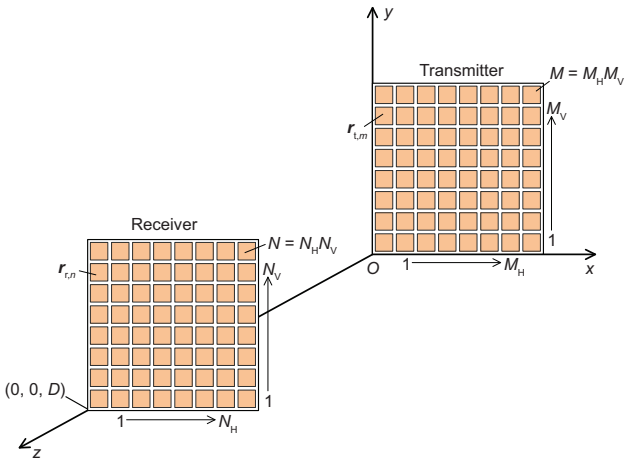

Fig. 1 Illustration of the investigated XL-MIMO system

Similarly, for the receiver equipped with a UPA, let N_{V}, $\Delta_{\mathrm{r,V}}$, and $L_{\mathrm{r,V}} = N_{\mathrm{V}}\Delta_{\mathrm{r,V}}$ denote the number of antennas per column, the vertical antenna spacing, and the vertical side length, respectively. Moreover, we denote the number of antennas per row, the horizontal antenna spacing, and the horizontal side length as N_{H}, $\Delta_{\mathrm{r,H}}$, and $L_{\mathrm{r,H}} = N_{\mathrm{H}}\Delta_{\mathrm{r,H}}$, respectively. The receiver is equipped with $N = N_{\mathrm{H}}N_{\mathrm{V}}$ antennas, which are also indexed row by row as $n \in \{1, 2, \ldots, N\}$ based on the same indexing principle as the transmitter. Thus, the location of the n^{th} antenna element at the receiver can be represented as $\boldsymbol{r}_{\mathrm{r},n} = [t(n)\Delta_{\mathrm{r,H}}, k(n)\Delta_{\mathrm{r,V}}, D]^{\mathrm{T}} \in \mathbb{R}^3$, where $t(n) = \mathrm{mod}(n-1, N_{\mathrm{H}})$ and $k(n) = \lfloor (n-1)/N_{\mathrm{H}} \rfloor$ are the horizontal and vertical indices of the n^{th} antenna element at the receiver, respectively. Moreover, D is the distance between the left-bottom antenna element of the transmitter and the left-bottom antenna element of the receiver.

2.1.2 Scalar Green channel model

The channel based on the scalar Green function between a particular receiving point $\boldsymbol{r}_{\mathrm{r}} \in \mathbb{R}^3$ and a particular transmitting point $\boldsymbol{r}_{\mathrm{t}} \in \mathbb{R}^3$ can be denoted by (Yuan et al., 2022)

$$G(\boldsymbol{r}_{\mathrm{r}}, \boldsymbol{r}_{\mathrm{t}}) = \frac{1}{4\pi} \frac{\exp(-\mathrm{j}\kappa_0 \|\boldsymbol{r}_{\mathrm{r}} - \boldsymbol{r}_{\mathrm{t}}\|)}{\|\boldsymbol{r}_{\mathrm{r}} - \boldsymbol{r}_{\mathrm{t}}\|}, \quad (1)$$

where $\kappa_0 = 2\pi/\lambda$ is the wavenumber and λ is the wavelength. For the UPA-based XL-MIMO system, the channel matrix generated by the scalar Green function between the receiver with N antennas and the transmitter with M antennas can be denoted as $\boldsymbol{H}_{\mathrm{S}} \in \mathbb{C}^{N \times M}$, whose $(n, m)^{\mathrm{th}}$ element, $[\boldsymbol{H}_{\mathrm{S}}]_{nm} = G_{nm}$, is the scalar Green function between the n^{th} receiving antenna and m^{th} transmitting antenna, defined as (Yuan et al., 2022)

$$G_{nm} = G(\boldsymbol{r}_{\mathrm{r},n}, \boldsymbol{r}_{\mathrm{t},m}) = \frac{1}{4\pi} \frac{\exp(-\mathrm{j}\kappa_0 d_{nm})}{d_{nm}}, \quad (2)$$

where $\boldsymbol{r}_{\mathrm{r},n} \in \mathbb{R}^3$ is the location of the n^{th} receiving antenna, $\boldsymbol{r}_{\mathrm{t},m} \in \mathbb{R}^3$ is the location of the m^{th}

transmitting antenna, and $d_{nm}=\|\boldsymbol{r}_{\mathrm{r},n}-\boldsymbol{r}_{\mathrm{t},m}\|$ is the distance between the n^{th} receiving antenna and the m^{th} transmitting antenna.

2.1.3 Dyadic Green channel model

Note that the scalar Green function omits the polarization effect, which would have a great effect on the system performance in near-field communications (Yuan et al., 2022; Wei et al., 2023; Wang et al., 2024b). To capture full polarization effects, the dyadic Green function can be applied. Specifically, the dyadic Green function between a particular receiving point $\boldsymbol{r}_{\mathrm{r}}\in\mathbb{R}^3$ and a particular transmitting point $\boldsymbol{r}_{\mathrm{t}}\in\mathbb{R}^3$ can be denoted by $\boldsymbol{G}\left(\boldsymbol{r}_{\mathrm{r}},\boldsymbol{r}_{\mathrm{t}}\right)\in\mathbb{C}^{3\times3}$, defined as

$$\boldsymbol{G}\left(\boldsymbol{r}_{\mathrm{r}},\boldsymbol{r}_{\mathrm{t}}\right)=\left(\boldsymbol{I}_3+\frac{\nabla_{\boldsymbol{r}_{\mathrm{r}}}\nabla_{\boldsymbol{r}_{\mathrm{r}}}^{\mathrm{H}}}{\kappa_0^2}\right)G\left(\boldsymbol{r}_{\mathrm{r}},\boldsymbol{r}_{\mathrm{t}}\right),\tag{3}$$

where $G\left(\boldsymbol{r}_{\mathrm{r}},\boldsymbol{r}_{\mathrm{t}}\right)$ is the scalar Green function based channel matrix between $\boldsymbol{r}_{\mathrm{r}}$ and $\boldsymbol{r}_{\mathrm{t}}$ given as Eq. (1) (Arnoldus, 2001; Wei et al., 2023; Lei et al., 2024a).

As observed in Eq. (3), the dyadic Green channel $\boldsymbol{G}\left(\boldsymbol{r}_{\mathrm{r}},\boldsymbol{r}_{\mathrm{t}}\right)$ can be derived by scaling the scalar Green channel $G\left(\boldsymbol{r}_{\mathrm{r}},\boldsymbol{r}_{\mathrm{t}}\right)$ with the operator $\left(\boldsymbol{I}_3+\frac{\nabla_{\boldsymbol{r}_{\mathrm{r}}}\nabla_{\boldsymbol{r}_{\mathrm{r}}}^{\mathrm{H}}}{\kappa_0^2}\right)$. An arbitrary dyadic Green function $\boldsymbol{G}\in\mathbb{C}^{3\times3}$ can be written in a matrix form with the $(p,q)^{\mathrm{th}}$ element G^{pq} being the scalar Green function between the p^{th} polarization of the receiving point and the q^{th} polarization of the transmitting source point, where $p,q\in\{x,y,z\}$. Thus, the dyadic Green channel between the receiver with N antennas and the transmitter with M antennas can be denoted by $\boldsymbol{H}_{\mathrm{D}}\in\mathbb{C}^{3N\times3M}$:

$$\boldsymbol{H}_{\mathrm{D}}=\begin{bmatrix}\boldsymbol{H}^{xx}&\boldsymbol{H}^{xy}&\boldsymbol{H}^{xz}\\\boldsymbol{H}^{yx}&\boldsymbol{H}^{yy}&\boldsymbol{H}^{yz}\\\boldsymbol{H}^{zx}&\boldsymbol{H}^{zy}&\boldsymbol{H}^{zz}\end{bmatrix},\tag{4}$$

where $\boldsymbol{H}^{pq}\in\mathbb{C}^{N\times M}$ is the scalar Green function channel matrix between the p^{th} polarization of the receiver with N antennas and the q^{th} polarization of the transmitter with M antennas. $\boldsymbol{H}^{pq}\in\mathbb{C}^{N\times M}$ can be further represented in the matrix form as

$$\boldsymbol{H}^{pq}=\begin{bmatrix}G_{11}^{pq}&G_{12}^{pq}&\cdots&G_{1M}^{pq}\\G_{21}^{pq}&G_{22}^{pq}&\cdots&G_{2M}^{pq}\\\vdots&\vdots&&\vdots\\G_{N1}^{pq}&G_{N2}^{pq}&\cdots&G_{NM}^{pq}\end{bmatrix},\tag{5}$$

where $\left[\boldsymbol{H}^{pq}\right]_{nm}=G_{nm}^{pq}$ is the $(p,q)^{\mathrm{th}}$ element of the dyadic Green function between the n^{th} receiving antenna and the m^{th} transmitting antenna $\boldsymbol{G}\left(\boldsymbol{r}_{\mathrm{r},n},\boldsymbol{r}_{\mathrm{t},m}\right)$, defined as

$$\boldsymbol{G}(\boldsymbol{r}_{\mathrm{r},n},\boldsymbol{r}_{\mathrm{t},m})=\frac{1}{4\pi}\left(\boldsymbol{I}_3+\frac{\nabla_{\boldsymbol{r}_{\mathrm{r},n}}\nabla_{\boldsymbol{r}_{\mathrm{r},n}}^{\mathrm{H}}}{\kappa_0^2}\right)G(\boldsymbol{r}_{\mathrm{r},n},\boldsymbol{r}_{\mathrm{t},m}).\tag{6}$$

2.2 CAP plane based XL-MIMO

2.2.1 System feature

As for the CAP plane based XL-MIMO system, we consider a scenario with both a transmitter and a receiver equipped with a 2D CAP plane, where the transmitter is located in the XY plane with its left-bottom point being the origin. Correspondingly, the vertical and horizontal side lengths for the transmitter are $L_{\mathrm{t,V}}$ and $L_{\mathrm{t,H}}$, respectively. $L_{\mathrm{r,V}}$ and $L_{\mathrm{r,H}}$ are the vertical and horizontal side lengths for the receiver, respectively. Moreover, the distance between the left-bottom points of the transmitter and the receiver is D. Let S_{R} and S_{T} denote the receiving CAP region and the transmitting CAP region, respectively. For the ease of EDoF analysis in the following, we define variables such as the side length and the locations of transmitting/receiving points similar to those of the UPA system. However, all the analysis frameworks introduced in this paper hold for arbitrary parameter settings instead of limiting the variables in the CAP system similar to that of the UPA system.

2.2.2 Green function based channel

Note that the 2D CAP planes show continuous features. For the scalar Green channel model, the channel between a particular receiving point $\boldsymbol{r}_{\mathrm{r}}\in\mathbb{R}^3$ in S_{R} and a particular transmitting point $\boldsymbol{r}_{\mathrm{t}}\in\mathbb{R}^3$ in S_{T} can be denoted by $G\left(\boldsymbol{r}_{\mathrm{r}},\boldsymbol{r}_{\mathrm{t}}\right)$ by substituting respective coordinates into Eq. (1). Moreover, the dyadic Green channel $\boldsymbol{G}\left(\boldsymbol{r}_{\mathrm{r}},\boldsymbol{r}_{\mathrm{t}}\right)\in\mathbb{C}^{3\times3}$ for a particular receiving point $\boldsymbol{r}_{\mathrm{r}}\in\mathbb{R}^3$ in S_{R} and a particular transmitting point $\boldsymbol{r}_{\mathrm{t}}\in\mathbb{R}^3$ in S_{T} can be computed by substituting respective coordinates into Eq. (3).

3 EDoF analysis

In this section, we construct the EDoF performance analysis framework for the 2D CAP plane

systems over both the scalar and dyadic Green channels. To maintain integrity, we first briefly introduce the EDoF analysis framework for the UPA system.

3.1 UPA-based XL-MIMO

3.1.1 Scalar Green channel model

For the UPA system with the scalar Green channel given as Eq. (4), the EDoF ε_{S} can be approximately computed as (Yuan et al., 2022; Ouyang et al., 2023)

$$\varepsilon_{\mathrm{S}}=\frac{\mathrm{tr}^2\left(\boldsymbol{R}_{\mathrm{S}}\right)}{\left\|\boldsymbol{R}_{\mathrm{S}}\right\|_{\mathrm{F}}^2}, \tag{7}$$

where $\boldsymbol{R}_{\mathrm{S}}=\boldsymbol{H}_{\mathrm{S}}^{\mathrm{H}}\boldsymbol{H}_{\mathrm{S}}\in\mathbb{C}^{M\times M}$ is the correlation matrix for the scalar Green channel.

3.1.2 Dyadic Green channel model

For the dyadic Green channel given in Eq. (4), the EDoF ε_{D} can be approximated as

$$\varepsilon_{\mathrm{D}}=\frac{\mathrm{tr}^2\left(\boldsymbol{R}_{\mathrm{D}}\right)}{\left\|\boldsymbol{R}_{\mathrm{D}}\right\|_{\mathrm{F}}^2}, \tag{8}$$

where $\boldsymbol{R}_{\mathrm{D}}=\boldsymbol{H}_{\mathrm{D}}^{\mathrm{H}}\boldsymbol{H}_{\mathrm{D}}\in\mathbb{C}^{3M\times 3M}$ is the correlation matrix for the dyadic Green channel.

3.2 CAP plane based XL-MIMO

3.2.1 Scalar Green channel model

For CAP plane based XL-MIMO, the EDoF performance analysis framework, which is different from that of the UPA-based XL-MIMO system, should be implemented due to its continuous array aperture. From the mathematical vision, the CAP plane based system can be viewed as a special case of the UPA-based system, assuming an infinite number of antennas while maintaining the physical array size. However, it is not convenient or technically sound to evaluate the EDoF performance for the CAP plane based system based on the EDoF performance analysis framework for the UPA-based system by considering an infinite number of antennas. This is because the channel matrices would be of infinitely high dimension, leading to extremely high computational complexity, and the EDoF results are also not intuitive for obtaining technical insights into the EDoF performance analysis for the CAP-based system. Thus, it is vital to derive a tailored EDoF performance analysis framework for the CAP-based system. Notably, the auto-correlation kernel $K(\boldsymbol{r}_{\mathrm{t}},\boldsymbol{r}_{\mathrm{t}'})$ is defined to indicate the correlation characteristic between two transmitting points in the transmitting region S_{T} for $\boldsymbol{r}_{\mathrm{t}}\in S_{\mathrm{T}}$, $\boldsymbol{r}_{\mathrm{t}'}\in S_{\mathrm{T}}$ over the scalar Green channel as follows (Jiang and Gao, 2023):

$$K(\boldsymbol{r}_{\mathrm{t}},\boldsymbol{r}_{\mathrm{t}'})=\int_{S_{\mathrm{R}}}G^{*}\left(\boldsymbol{r}_{\mathrm{r}},\boldsymbol{r}_{\mathrm{t}}\right)G\left(\boldsymbol{r}_{\mathrm{r}},\boldsymbol{r}_{\mathrm{t}'}\right)\mathrm{d}\boldsymbol{r}_{\mathrm{r}}, \tag{9}$$

where $G\left(\boldsymbol{r}_{\mathrm{r}},\boldsymbol{r}_{\mathrm{t}}\right)$ is the scalar Green channel between the transmitting point $\boldsymbol{r}_{\mathrm{t}}$ and the receiving point $\boldsymbol{r}_{\mathrm{r}}$. Note that the $(m_1,m_2)^{\mathrm{th}}$ element of the correlation matrix $\boldsymbol{R}_{\mathrm{S}}$ can be computed as

$$\left[\boldsymbol{R}_{\mathrm{S}}\right]_{m_1m_2}=\sum_{n=1}^{N}G_{nm_1}^{*}G_{nm_2}, \tag{10}$$

where G_{nm_1} and G_{nm_2} can be calculated as in Eq. (2). Then, $\mathrm{tr}\left(\boldsymbol{R}_{\mathrm{S}}\right)$ and $\left\|\boldsymbol{R}_{\mathrm{S}}\right\|_{\mathrm{F}}^2$ in Eq. (7) can be further written as in Eq. (11) (see the bottom of this page).

Then, by applying the asymptotic analysis for Eq. (11) with the invariant array physical size over $M\to\infty$, $N\to\infty$, $\left[\boldsymbol{R}_{\mathrm{S}}\right]_{m_1m_2}$, $\mathrm{tr}\left(\boldsymbol{R}_{\mathrm{S}}\right)$, and $\left\|\boldsymbol{R}_{\mathrm{S}}\right\|_{\mathrm{F}}^2$ can be asymptotically represented as in Eq. (12) (see the bottom of this page), according to the asymptotic representation (Jiang and Gao, 2023)

$$\begin{cases}\mathrm{d}\boldsymbol{r}_{\mathrm{r}}=\mathrm{d}y_{\mathrm{r}}\mathrm{d}z_{\mathrm{r}}\to\frac{L_{\mathrm{r,H}}L_{\mathrm{r,V}}}{N_{\mathrm{H}}N_{\mathrm{V}}},\\ \mathrm{d}\boldsymbol{r}_{\mathrm{t}}=\mathrm{d}y_{\mathrm{t}}\mathrm{d}z_{\mathrm{t}}\to\frac{L_{\mathrm{t,H}}L_{\mathrm{t,V}}}{M_{\mathrm{H}}M_{\mathrm{V}}},\\ \mathrm{d}\boldsymbol{r}_{\mathrm{t}'}=\mathrm{d}y_{\mathrm{t}'}\mathrm{d}z_{\mathrm{t}'}\to\frac{L_{\mathrm{t,H}}L_{\mathrm{t,V}}}{M_{\mathrm{H}}M_{\mathrm{V}}}.\end{cases} \tag{13}$$

$$\begin{cases}\mathrm{tr}\left(\boldsymbol{R}_{\mathrm{S}}\right)=\sum_{m=1}^{M}\sum_{n=1}^{N}\left[\boldsymbol{R}_{\mathrm{S}}\right]_{mm}^2=\sum_{m=1}^{M}\sum_{n=1}^{N}\left|G_{nm}\right|^2,\\ \left\|\boldsymbol{R}_{\mathrm{S}}\right\|_{\mathrm{F}}^2=\sum_{m_1=1}^{M}\sum_{m_2=1}^{N}\left[\boldsymbol{R}_{\mathrm{S}}\right]_{m_1m_2}^2=\sum_{m_1=1}^{M}\sum_{m_2=1}^{N}\left|\sum_{n=1}^{N}G_{nm_1}^{*}G_{nm_2}\right|^2.\end{cases} \tag{11}$$

$$\begin{cases}\left[\boldsymbol{R}_{\mathrm{S}}\right]_{m_1m_2}\to\frac{N_{\mathrm{H}}N_{\mathrm{V}}}{L_{\mathrm{r,H}}L_{\mathrm{r,V}}}K(\boldsymbol{r}_{\mathrm{t}},\boldsymbol{r}_{\mathrm{t}'}),\\ \mathrm{tr}\left(\boldsymbol{R}_{\mathrm{S}}\right)\to\frac{N_{\mathrm{H}}N_{\mathrm{V}}M_{\mathrm{H}}M_{\mathrm{V}}}{L_{\mathrm{r,H}}L_{\mathrm{r,V}}L_{\mathrm{t,H}}L_{\mathrm{t,V}}}\int_{S_{\mathrm{T}}}\int_{S_{\mathrm{R}}}\left|G\left(\boldsymbol{r}_{\mathrm{r}},\boldsymbol{r}_{\mathrm{t}}\right)\right|^2\mathrm{d}\boldsymbol{r}_{\mathrm{r}}\mathrm{d}\boldsymbol{r}_{\mathrm{t}},\\ \left\|\boldsymbol{R}_{\mathrm{S}}\right\|_{\mathrm{F}}^2\to\frac{(N_{\mathrm{H}}N_{\mathrm{V}}M_{\mathrm{H}}M_{\mathrm{V}})^2}{(L_{\mathrm{r,H}}L_{\mathrm{r,V}}L_{\mathrm{t,H}}L_{\mathrm{t,V}})^2}\int_{S_{\mathrm{T}}}\int_{S_{\mathrm{T}}}\left|K(\boldsymbol{r}_{\mathrm{t}},\boldsymbol{r}_{\mathrm{t}'})\right|^2\mathrm{d}\boldsymbol{r}_{\mathrm{t}}\mathrm{d}\boldsymbol{r}_{\mathrm{t}'}.\end{cases} \tag{12}$$

Based on the above derivations, the EDoF for the CAP system over the scalar Green channel can be derived as in the following theorem:

Theorem 1 For the CAP-based XL-MIMO system over the scalar Green channel, by applying the asymptotic analysis for Eq. (7) with the invariant array physical size over $M \to \infty$, $N \to \infty$, we can compute the EDoF performance as

$$\Psi_{\mathrm{S}} = \frac{\left(\int_{S_{\mathrm{T}}}\int_{S_{\mathrm{R}}} \left|G\left(\boldsymbol{r}_{\mathrm{r}}, \boldsymbol{r}_{\mathrm{t}}\right)\right|^2 \mathrm{d}\boldsymbol{r}_{\mathrm{r}}\mathrm{d}\boldsymbol{r}_{\mathrm{t}}\right)^2}{\int_{S_{\mathrm{T}}}\int_{S_{\mathrm{T}}} \left|K(\boldsymbol{r}_{\mathrm{t}}, \boldsymbol{r}_{\mathrm{t}'})\right|^2 \mathrm{d}\boldsymbol{r}_{\mathrm{t}}\mathrm{d}\boldsymbol{r}_{\mathrm{t}'}}. \tag{14}$$

3.2.2 Dyadic Green channel model

For the CAP system over the dyadic Green channel, motivated by the above analysis of the scalar Green channel model, we also start from the correlation matrix $\boldsymbol{R}_{\mathrm{D}}$ and dyadic Green channel $\boldsymbol{H}_{\mathrm{D}}$ for the UPA system.

Relying on the structure of $\boldsymbol{H}_{\mathrm{D}}$ given in Eq. (4), for the ease of representation, we denote the polarization subscripts as $x \to 1$, $y \to 2$, and $z \to 3$, respectively. Based on Eq. (4), the $(c,d)^{\mathrm{th}}$ element of $\boldsymbol{R}_{\mathrm{D}} \in \mathbb{C}^{3M\times 3M}$ can be constructed as

$$\left[\boldsymbol{R}_{\mathrm{D}}\right]_{cd} = \sum_{i=1}^{3}\sum_{n=1}^{N}\left(G_{na}^{ip}\right)^{*} G_{nb}^{iq}, \tag{15}$$

where G_{na}^{ip} is the $(i,p)^{\mathrm{th}}$ element of the dyadic Green function between the n^{th} receiving antenna and the a^{th} transmitting antenna $\boldsymbol{G}\left(\boldsymbol{r}_{\mathrm{r},n}, \boldsymbol{r}_{\mathrm{t},a}\right)$, as defined in Eq. (6), with $a = 1,2,\ldots,M$, $b = 1,2,\ldots,M$, $\{p,q\} \in \{1,2,3\}$, $c = (p-1)M + a$, and $d = (q-1)M + b$.

Furthermore, $\mathrm{tr}\left(\boldsymbol{R}_{\mathrm{D}}\right)$ and $\left\|\boldsymbol{R}_{\mathrm{D}}\right\|_{\mathrm{F}}^2$ in Eq. (8) can be expanded as Eq. (16) (see the bottom of this page) according to Eq. (15). Note that the diagonal elements of $\boldsymbol{R}_{\mathrm{D}}$ are derived by letting $c = d$ in $\left[\boldsymbol{R}_{\mathrm{D}}\right]_{cd}$ as

$$(p-1)M + a = (q-1)M + b, \tag{17}$$

which holds only under the conditions $p = q$ and $a = b$. This can be easily proven based on the value ranges of these variables. Thus, we can write $\mathrm{tr}\left(\boldsymbol{R}_{\mathrm{D}}\right)$ as in Eq. (16) by letting $p = q$ and $a = b$ to compute $\left[\boldsymbol{R}_{\mathrm{D}}\right]_{cc}$. Note that the polarization effect can be clearly observed in the expanded form of Eq. (8) as in Eq. (16).

Then, we define the polarized auto-correlation kernel to describe the correlation characteristic between two particular transmitting points in S_{T} for $\boldsymbol{r}_{\mathrm{t}} \in S_{\mathrm{T}}$ and $\boldsymbol{r}_{t'} \in S_{\mathrm{T}}$, over a particular polarization direction pair $\{p,q\} \in \{1,2,3\}$:

$$\bar{K}(\boldsymbol{r}_{\mathrm{t}}, \boldsymbol{r}_{\mathrm{t}'}, p, q) = \sum_{i=1}^{3}\int_{S_{\mathrm{R}}}\left[G^{ip}(\boldsymbol{r}_{\mathrm{r}}, \boldsymbol{r}_{\mathrm{t}})\right]^{*} G^{iq}\left(\boldsymbol{r}_{\mathrm{r}}, \boldsymbol{r}_{\mathrm{t}'}\right)\mathrm{d}\boldsymbol{r}_{\mathrm{r}}, \tag{18}$$

where $G^{ip}\left(\boldsymbol{r}_{\mathrm{r}}, \boldsymbol{r}_{\mathrm{t}}\right)$ is the $(i,p)^{\mathrm{th}}$ element of the dyadic Green channel between $\boldsymbol{r}_{\mathrm{r}} \in S_{\mathrm{R}}$ and $\boldsymbol{r}_{\mathrm{t}} \in S_{\mathrm{T}}$. Compared with the auto-correlation kernel function for the scalar Green channel in Eq. (9), the polarized auto-correlation kernel function in Eq. (18) can capture the polarization effect for a particular polarization direction pair $\{p,q\} \in \{1,2,3\}$, which can provide fundamentals for the EDoF performance computation for the CAP system over the dyadic Green channel with polarization.

Under the asymptotic condition $M \to \infty$, $N \to \infty$ with the invariant array physical size, we can obtain the asymptotic form of $\mathrm{tr}\left(\boldsymbol{R}_{\mathrm{D}}\right)$ and $\left\|\boldsymbol{R}_{\mathrm{D}}\right\|_{\mathrm{F}}^2$ as Eq. (19) (see the top of the next page) by applying similar asymptotic representations of $\mathrm{d}\boldsymbol{r}_{\mathrm{r}}$, $\mathrm{d}\boldsymbol{r}_{\mathrm{t}}$, and $\mathrm{d}\boldsymbol{r}_{\mathrm{t}'}$ as in Eq. (13). As observed in Eq. (19), compared with Eq. (12), the asymptotic representations of $\mathrm{tr}\left(\boldsymbol{R}_{\mathrm{D}}\right)$ and $\left\|\boldsymbol{R}_{\mathrm{D}}\right\|_{\mathrm{F}}^2$ capture the polarization effects by considering all possible polarization direction pairs $\{p,q\} \in \{1,2,3\}$, with the aid of the polarized auto-correlation kernel function defined in Eq. (18).

Thus, based on the above derivations, the EDoF performance for the CAP plane system with the dyadic Green channel can be derived as follows:

Theorem 2 For the CAP plane system based on the dyadic Green channel, by applying the asymptotic analysis for Eq. (7) over $M \to \infty$, $N \to \infty$ with the invariant array physical size, the EDoF can be calculated as

$$\Psi_{\mathrm{D}} = \frac{\left(\sum_{i=1}^{3}\sum_{p=1}^{3}\int_{S_{\mathrm{T}}}\int_{S_{\mathrm{R}}}\left|G^{ip}\left(\boldsymbol{r}_{\mathrm{r}}, \boldsymbol{r}_{\mathrm{t}}\right)\right|^2 \mathrm{d}\boldsymbol{r}_{\mathrm{r}}\mathrm{d}\boldsymbol{r}_{\mathrm{t}}\right)^2}{\sum_{p=1}^{3}\sum_{q=1}^{3}\int_{S_{\mathrm{T}}}\int_{S_{\mathrm{T}}}\left|\bar{K}(\boldsymbol{r}_{\mathrm{t}}, \boldsymbol{r}_{\mathrm{t}'}, p, q)\right|^2 \mathrm{d}\boldsymbol{r}_{\mathrm{t}}\mathrm{d}\boldsymbol{r}_{\mathrm{t}'}}. \tag{20}$$

$$\begin{cases} \mathrm{tr}\left(\boldsymbol{R}_{\mathrm{D}}\right) = \sum_{c=1}^{3M}\left[\boldsymbol{R}_{\mathrm{D}}\right]_{cc} = \sum_{p=1}^{3}\sum_{i=1}^{3}\sum_{a=1}^{M}\sum_{n=1}^{N}\left|G_{na}^{ip}\right|^2, \\ \left\|\boldsymbol{R}_{\mathrm{D}}\right\|_{\mathrm{F}}^2 = \sum_{c=1}^{3M}\sum_{d=1}^{3M}\left|\left[\boldsymbol{R}_{\mathrm{D}}\right]_{cd}\right|^2 = \sum_{p=1}^{3}\sum_{q=1}^{3}\sum_{a=1}^{M}\sum_{b=1}^{M}\left|\sum_{i=1}^{3}\sum_{n=1}^{N}\left(G_{na}^{ip}\right)^{*} G_{nb}^{iq}\right|^2. \end{cases} \tag{16}$$

$$\begin{cases} \mathrm{tr}\left(\boldsymbol{R}_{\mathrm{D}}\right) \to \frac{N_{\mathrm{H}}N_{\mathrm{V}}M_{\mathrm{H}}M_{\mathrm{V}}}{L_{\mathrm{r,H}}L_{\mathrm{r,V}}L_{\mathrm{t,H}}L_{\mathrm{t,V}}} \sum_{p=1}^{3}\sum_{i=1}^{3}\int_{S_{\mathrm{T}}}\int_{S_{\mathrm{R}}}\left|G^{ip}\left(\boldsymbol{r}_{\mathrm{r}},\boldsymbol{r}_{\mathrm{t}}\right)\right|^2 \mathrm{d}\boldsymbol{r}_{\mathrm{r}}\mathrm{d}\boldsymbol{r}_{\mathrm{t}}, \\ \left\|\boldsymbol{R}_{\mathrm{D}}\right\|_{\mathrm{F}}^2 \to \left(\frac{N_{\mathrm{H}}N_{\mathrm{V}}M_{\mathrm{H}}M_{\mathrm{V}}}{L_{\mathrm{r,H}}L_{\mathrm{r,V}}L_{\mathrm{t,H}}L_{\mathrm{t,V}}}\right)^2 \sum_{p=1}^{3}\sum_{q=1}^{3}\int_{S_{\mathrm{T}}}\int_{S_{\mathrm{T}}}\left|\bar{K}(\boldsymbol{r}_{\mathrm{t}},\boldsymbol{r}_{\mathrm{t}'},p,q)\right|^2 \mathrm{d}\boldsymbol{r}_{\mathrm{t}}\mathrm{d}\boldsymbol{r}_{\mathrm{t}'}. \end{cases} \tag{19}$$

In this section, we have provided the EDoF performance analysis frameworks for two plane based XL-MIMO hardware designs, i.e., UPA-based and 2D CAP plane based systems, over two near-field Green function based channel models, i.e., scalar and dyadic Green function based models. The EDoF performance frameworks in this section are available for the scenario with one transmitting plane and one receiving plane with any antenna array aperture sizes. The EDoF performance analysis for the scenarios with multiple transmitting or receiving planes is anticipated to be further conducted based on the fundamental frameworks considered in this paper.

4 Numerical results

In this study, we consider the square UPA and 2D CAP plane XL-MIMO systems, where $L_{\mathrm{t,V}} = L_{\mathrm{t,H}}$ and $L_{\mathrm{r,V}} = L_{\mathrm{r,H}}$. The number of antennas per side length in the UPA is equal, that is, $M_{\mathrm{V}} = M_{\mathrm{H}}$ and $N_{\mathrm{V}} = N_{\mathrm{H}}$. For ease of representation, let L_{t} and L_{r} denote the side lengths of the transmitting plane and the receiving plane, respectively. The carrier frequency is 3 GHz.

Fig. 2 investigates the EDoF performance for the UPA system versus the number of antennas per side with different side lengths. As observed, with the increase in the number of antennas, the EDoF would first increase and then reach an approximately saturated performance. Moreover, for a fixed transmitting distance, increasing the physical size of the transceiver can undoubtedly increase the EDoF performance. For instance, the scenario with $L_{\mathrm{t}} = L_{\mathrm{r}} = 18\lambda$ can achieve about 89.4% EDoF improvement compared with the scenario with $L_{\mathrm{t}} = L_{\mathrm{r}} = 15\lambda$. When the physical size of the transceiver increases, the number of antennas that achieves approximately saturated EDoF performance would also increase.

Fig. 3 analyzes the EDoF performance for the UPA system as a function of the number of antennas per side, considering different lengths of the receiving side. The figure reveals that for a fixed transmitting array aperture size, the EDoF performance benefits from a larger receiving array aperture size. For instance, about 94.4% EDoF improvement can be achieved for $L_{\mathrm{r}} = 6\lambda$ compared with $L_{\mathrm{r}} = 4\lambda$. Moreover, as the receiving array aperture size increases, the number of antennas required to achieve nearly optimal EDoF performance increases. More simulation results can be found in the supplementary materials.

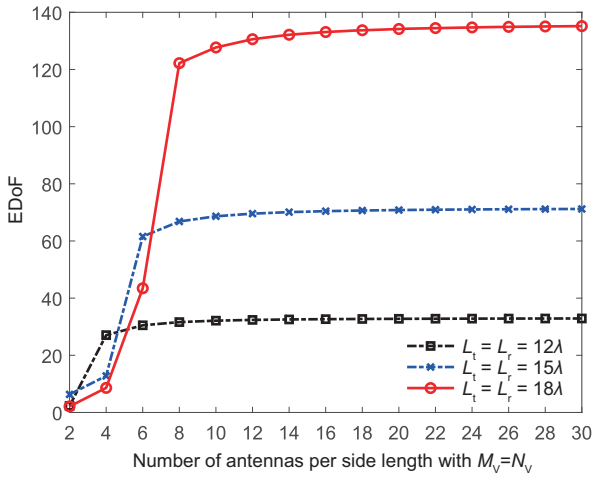

Fig. 2 EDoF performance for the UPA system versus the number of antennas per side with different side lengths over the dyadic Green channel ($L_{\mathrm{t}} = L_{\mathrm{r}}$ and $D = 40\lambda$)

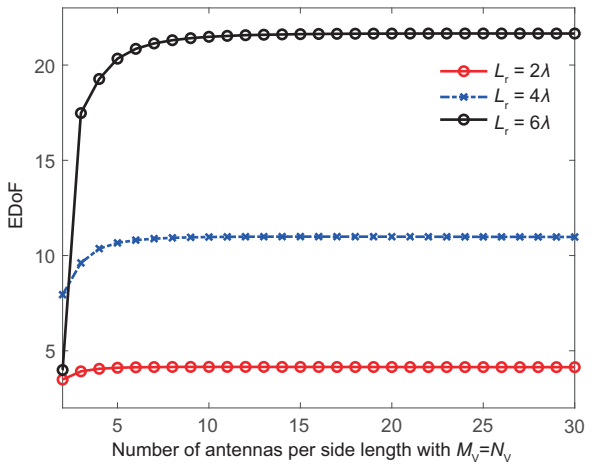

Fig. 3 EDoF performance for the UPA system versus the number of antennas per side with different lengths of the receiving side over the dyadic Green channel ($L_{\mathrm{t}} = 20\lambda$ and $D = 40\lambda$)

5 Conclusions

In this study, we carried out the EDoF performance analysis for the UPA and the 2D CAP systems. More importantly, the scalar and dyadic Green near-field channels were considered. First, we derived the EDoF performance for the UPA system by using discrete channel matrices based on either the scalar or dyadic Green function. For the 2D CAP plane system, asymptotic analysis was applied to construct the EDoF performance analysis framework based on the scalar or dyadic Green channel. For the numerical results, we presented a comparative analysis of the EDoF performance between the UPA-based and 2D CAP plane based XL-MIMO systems. We analyzed the effect of polarization and the physical size of the transceiver. It was observed that, with an increasing number of antennas, the EDoF performance of the UPA system would approach that of the 2D CAP plane system. Moreover, the EDoF performance benefits from the polarization and the physical size of the transceiver. Future studies are anticipated to further explore the EDoF analysis for three-dimensional antenna array structures as in Yuan et al. (2024).

Contributors

Zhe WANG and Jiayi ZHANG designed the research. Wenhui YI processed the data. Zhe WANG drafted the paper. Huahua XIAO and Dusit NIYATO helped organize the paper. Jiayi ZHANG, Dusit NIYATO, and Bo AI revised and finalized the paper.

Conflict of interest

All the authors declare that they have no conflict of interest.

Data availability

The data that support the findings of this study are available from the corresponding author upon reasonable request.

References

Arnoldus HF, 2001. Representation of the near-field, middle-field, and far-field electromagnetic Green's functions in reciprocal space. *J Opt Soc Am B*, 18(4):547-555. https://doi.org/10.1364/JOSAB.18.000547

Björnson E, Sanguinetti L, Wymeersch H, et al., 2019. Massive MIMO is a reality—what is next?: five promising research directions for antenna arrays. *Dig Signal Process*, 94:3-20. https://doi.org/10.1016/j.dsp.2019.06.007

Björnson E, Chae CB, Heath RWJr, et al., 2024. Towards 6G MIMO: massive spatial multiplexing, dense arrays, and interplay between electromagnetics and processing. https://doi.org/10.48550/arXiv.2401.02844

Chen SF, Zhang JY, Björnson E, et al., 2021. Structured massive access for scalable cell-free massive MIMO systems. *IEEE J Sel Areas Commun*, 39(4):1086-1100. https://doi.org/10.1109/JSAC.2020.3018836

Chen SF, Zhang JY, Björnson E, et al., 2023. Energy-efficient cell-free massive MIMO through sparse large-scale fading processing. *IEEE Trans Wirel Commun*, 22(12):9374-9389. https://doi.org/10.1109/TWC.2023.3270299

Cui MY, Dai LL, 2022. Channel estimation for extremely large-scale MIMO: far-field or near-field? *IEEE Trans Commun*, 70(4):2663-2677. https://doi.org/10.1109/TCOMM.2022.3146400

Cui MY, Wu ZD, Lu Y, et al., 2023. Near-field MIMO communications for 6G: fundamentals, challenges, potentials, and future directions. *IEEE Commun Mag*, 61(1):40-46. https://doi.org/10.1109/MCOM.004.2200136

Du HY, Wang JC, Niyato D, et al., 2023. Semantic communications for wireless sensing: RIS-aided encoding and self-supervised decoding. *IEEE J Sel Areas Commun*, 41(8):2547-2562. https://doi.org/10.1109/JSAC.2023.3288231

Du HY, Zhang RC, Liu YQ, et al., 2024. Enhancing deep reinforcement learning: a tutorial on generative diffusion models in network optimization. *IEEE Commun Surv Tut*, 26(4):2611-2646. https://doi.org/10.1109/COMST.2024.3400011

Gan X, Zhong CJ, Huang CW, et al., 2021. RIS-assisted multi-user MISO communications exploiting statistical CSI. *IEEE Trans Commun*, 69(10):6781-6792. https://doi.org/10.1109/TCOMM.2021.3100860

Gong TR, Gavriilidis P, Ji R, et al., 2024. Holographic MIMO communications: theoretical foundations, enabling technologies, and future directions. *IEEE Commun Surv Tut*, 26(1):196-257. https://doi.org/10.1109/COMST.2023.3309529

Huang CW, Yang ZH, Alexandropoulos GC, et al., 2021. Multi-hop RIS-empowered terahertz communications: a DRL-based hybrid beamforming design. *IEEE J Sel Areas Commun*, 39(6):1663-1677. https://doi.org/10.1109/JSAC.2021.3071836

Jiang YH, Gao FF, 2023. Electromagnetic channel model for near field MIMO systems in the half space. *IEEE Commun Lett*, 27(2):706-710. https://doi.org/10.1109/LCOMM.2022.3229445

Lei H, Zhang JY, Xiao HH, et al., 2024a. Channel estimation for XL-MIMO systems with polar-domain multi-scale residual dense network. *IEEE Trans Veh Technol*, 73(1):1479-1484. https://doi.org/10.1109/TVT.2023.3311010

Lei H, Zhang JY, Wang Z, et al., 2024b. Hybrid-field channel estimation for XL-MIMO systems with stochastic gradient pursuit algorithm. *IEEE Trans Signal Process*, 72:2998-3012. https://doi.org/10.1109/TSP.2024.3406348

Letaief KB, Chen W, Shi YM, et al., 2019. The roadmap to 6G: AI empowered wireless networks. *IEEE Commun*

Mag, 57(8):84-90. https://doi.org/10.1109/MCOM.2019.1900271

Liu YW, Ouyang CJ, Wang ZL, et al., 2024. Near-field communications: a comprehensive survey. https://doi.org/10.48550/arXiv.2401.05900

Liu ZH, Zhang JY, Liu ZL, et al., 2024. Double-layer power control for mobile cell-free XL-MIMO with multi-agent reinforcement learning. *IEEE Trans Wirel Commun*, 23(5):4658-4674. https://doi.org/10.1109/TWC.2023.3321334

Liu ZL, Zhang JY, Liu ZH, et al., 2024. Cell-free XL-MIMO meets multi-agent reinforcement learning: architectures, challenges, and future directions. *IEEE Wirel Commun*, 31(4):155-162. https://doi.org/10.1109/MWC.007.2300176

Lu HQ, Zeng Y, 2022. Communicating with extremely large-scale array/surface: unified modeling and performance analysis. *IEEE Trans Wirel Commun*, 21(6):4039-4053. https://doi.org/10.1109/TWC.2021.3126384

Lu HQ, Zeng Y, You CS, et al., 2023. A tutorial on near-field XL-MIMO communications towards 6G. https://doi.org/10.48550/arXiv.2310.11044

Marzetta TL, 2010. Noncooperative cellular wireless with unlimited numbers of base station antennas. *IEEE Trans Wirel Commun*, 9(11):3590-3600. https://doi.org/10.1109/TWC.2010.092810.091092

Ouyang CJ, Liu YW, Yang HW, 2022. Performance of downlink and uplink integrated sensing and communications (ISAC) systems. *IEEE Wirel Commun Lett*, 11(9):1850-1854. https://doi.org/10.1109/LWC.2022.3184409

Ouyang CJ, Liu YW, Zhang XQ, et al., 2023. Near-field communications: a degree-of-freedom perspective. https://doi.org/10.48550/arXiv.2308.00362

Shi EY, Zhang JY, Du HY, et al., 2024. RIS-aided cell-free massive MIMO systems for 6G: fundamentals, system design, and applications. *Proc IEEE*, 112(4):331-364. https://doi.org/10.1109/JPROC.2024.3404491

Sun G, He L, Sun ZM, et al., 2024. Joint task offloading and resource allocation in aerial-terrestrial UAV networks with edge and fog computing for post-disaster rescue. *IEEE Trans Mob Comput*, 23(9):8582-8600. https://doi.org/10.1109/TMC.2024.3350886

Tang P, Zhang JH, Miao HY, et al., 2024. XL-MIMO channel measurement, characterization, and modeling for 6G: a survey. *Front Inform Technol Electron Eng*, early access. https://doi.org/10.1631/FITEE.2400140

Tataria H, Shafi M, Molisch AF, et al., 2021. 6G wireless systems: vision, requirements, challenges, insights, and opportunities. *Proc IEEE*, 109(7):1166-1199. https://doi.org/10.1109/JPROC.2021.3061701

Wang Z, Zhang JY, Du HY, et al., 2024a. Extremely large-scale MIMO: fundamentals, challenges, solutions, and future directions. *IEEE Wirel Commun*, 31(3):117-124. https://doi.org/10.1109/MWC.132.2200443

Wang Z, Zhang JY, Du HY, et al., 2024b. A tutorial on extremely large-scale MIMO for 6G: fundamentals, signal processing, and applications. *IEEE Commun Surv Tut*, 26(3):1560-1605. https://doi.org/10.1109/COMST.2023.3349276

Wei L, Huang CW, Alexandropoulos GC, et al., 2023. Tripolarized holographic MIMO surfaces for near-field communications: channel modeling and precoding design. *IEEE Trans Wirel Commun*, 22(12):8828-8842. https://doi.org/10.1109/TWC.2023.3266298

Xie ZY, Liu YW, Xu JQ, et al., 2023. Performance analysis for near-field MIMO: discrete and continuous aperture antennas. *IEEE Wirel Commun Lett*, 12(12):2258-2262. https://doi.org/10.1109/LWC.2023.3317492

Xu BK, Zhang JY, Li JX, et al., 2023. Jac-PCG based low-complexity precoding for extremely large-scale MIMO systems. *IEEE Trans Veh Technol*, 72(12):16811-16816. https://doi.org/10.1109/TVT.2023.3293546

Xu BK, Zhang JY, Du HY, et al., 2024. Resource allocation for near-field communications: fundamentals, tools, and outlooks. *IEEE Wirel Commun*, 31(5):42-50. https://doi.org/10.1109/MWC.016.2300528

You CS, Zhang YP, Wu CY, et al., 2023. Near-field beam management for extremely large-scale array communications. https://doi.org/10.48550/arXiv.2306.16206

You XH, Wang CX, Huang J, et al., 2021. Towards 6G wireless communication networks: vision, enabling technologies, and new paradigm shifts. *Sci China Inform Sci*, 64(1):110301. https://doi.org/10.1007/s11432-020-2955-6

Yuan SSA, He Z, Chen XM, et al., 2022. Electromagnetic effective degree of freedom of an MIMO system in free space. *IEEE Antenn Wirel Propag Lett*, 21(3):446-450. https://doi.org/10.1109/LAWP.2021.3135018

Yuan SSA, Wu J, Xu HJ, et al., 2024. Breaking the degrees-of-freedom limit of holographic MIMO communications: a 3-D antenna array topology. *IEEE Trans Veh Technol*, 73(8):11276-11288. https://doi.org/10.1109/TVT.2024.3372704

Zhang JY, Björnson E, Matthaiou M, et al., 2020. Prospective multiple antenna technologies for beyond 5G. *IEEE J Sel Areas Commun*, 38(8):1637-1660. https://doi.org/10.1109/JSAC.2020.3000826

Zhang JY, Zhang J, Björnson E, et al., 2021. Local partial zero-forcing combining for cell-free massive MIMO systems. *IEEE Trans Commun*, 69(12):8459-8473. https://doi.org/10.1109/TCOMM.2021.3110214

Zhang ZJ, Dai LL, 2023. Pattern-division multiplexing for multi-user continuous-aperture MIMO. *IEEE J Sel Areas Commun*, 41(8):2350-2366. https://doi.org/10.1109/JSAC.2023.3288244

Zheng JK, Zhang JY, Cheng JL, et al., 2023. Asynchronous cell-free massive MIMO with rate-splitting. *IEEE J Sel Areas Commun*, 41(5):1366-1382. https://doi.org/10.1109/JSAC.2023.3240709

List of supplementary materials

Fig. S1 EDoF performance for the UPA system with $L_{\mathrm{t}} = L_{\mathrm{r}} = 8\lambda$ and the 2D CAP plane system over the dyadic Green channel

Fig. S2 EDoF performance against the transmitting distance D for the 2D CAP plane system over the dyadic Green channel with single, double, or triple polarization, with $L_{\mathrm{t}} = L_{\mathrm{r}} = 30\lambda$

Fig. S3 EDoF performance against the side length of the 2D CAP plane transmitting L_{t} over the dyadic Green channel with different values of the side length of the 2D CAP plane receiver, with $D = 13\lambda$